Letter

The electric form factor of the neutron and its chiral content

M.M. Kaskulov and P. Grabmayr[a]

Physikalisches Institut, Universität Tübingen, D-72076 Tübingen, Germany

Abstract. Considering the nucleon as a system of confined valence quarks surrounded by pions we derive a Galster-like parameterization of the neutron electric form factor G_E^n. Furthermore, we show that the proposed parameterization can be linked to properties of the pion cloud. By this, the high-quality data for the pion form factor can be used in predictions of G_E^n in the low-Q^2 region, where the direct double-polarization measurements are not available.

PACS. 13.40.Gp Electromagnetic form factors – 12.39.Jh Nonrelativistic quark model

The electromagnetic (e.m.) form factors of the nucleons contain all the information on the internal nucleon structure and in particular they are very sensitive to the details of the interaction between the valence quarks. Already the first analyses by Hofstadter *et al.* [1] demonstrated that the proton electric form factor can be described by a dipole-type form

$$G_D(Q^2) = (1 + Q^2/\Lambda^2)^{-2}. \qquad (1)$$

Using the canonical $\Lambda_D^2 = 0.71$ GeV^2, G_E^p is reproduced up to four-momentum transfer $Q^2 \sim 1$ GeV^2. Also the magnetic nucleon form factors, G_M^p and G_M^n, are reproduced reasonably well. Recently, new precise polarization experiments and new analyses [2–6] have brought clear evidence for the deviations of the form factors from the simple dipole form at high Q^2. Slight deviations from the dipole form at low Q^2 have been attributed to the underlying pionic and quarkonic structure of the nucleons [4].

The neutron electric form factor G_E^n is the most uncertain one due to its vanishing net charge and the absence of free neutron targets. The internal structure of the neutron is also reflected by a finite charge radius [7,8]. Understanding the measured $\langle r^2 \rangle_n = -0.115 \pm 0.003$ [9] is still an interesting goal, since the contributing Foldy term [8] of $3F_2(0)/2M_N^2 = -0.126$ fm^2 almost equals the measured $\langle r^2 \rangle_n$ value. At the same time, a recent analysis by Isgur [10] indicates that the Foldy term does not really explain the neutron charge radius and its charge distribution, because in leading order of the relativistic approximation to the constituent-quark model (CQM)

the Foldy term is canceled exactly by a contribution to the Dirac form factor F_1. This result was confirmed by ref. [11] where it was argued that both the success of the CQM in reproducing the ratio of the proton to neutron magnetic moments and the success of the Foldy term in reproducing the observed charge radius of the neutron are coincidental.

The extraction of the nonzero charge form factor G_E^n from elastic electron scattering off the deuteron is rather model dependent [1,12,13]. In recent years G_E^n has been studied successfully by double-polarization experiments [14] and the most recent parameterizations in the range up to $Q^2 \sim 1$ GeV^2 seem to converge [3–5,15,16]. The so-called Galster [12] parameterization of G_E^n is based on the same dipole form $G_D(Q^2)$ as for the proton. In oder to account for the condition $G_E^n(Q^2 = 0) = 0$ required by the vanishing charge of the neutron, G_D is multiplied by an appropriate function. Out of four trial functions [12],

$$G_E^n(Q^2) = \frac{a_G \tau}{1 + b_G \tau} \, G_D(Q^2) \qquad (2)$$

served best, where $\tau = Q^2/4M_n^2$ and $M_n = 0.939$ GeV^2 is the neutron mass. Originally [12], the parameter a_G was set equal to $-\mu_n$ and the fit to the data resulted in $b_G = 5.6$. More recent fits, *e.g.* ref. [4], obtain $a \sim 1.73$ which reproduces the measured root-mean-square radius of the neutron and determines $b = 4.62$.

Theoretically, up to now the Galster parameterization has no particular theoretical justification and is considered as a purely empirical description, *i.e.* a_G and b_G are fitting parameters. In this paper we wish to show that the parameterization of the neutron electric form factor G_E^n can be derived directly under certain assumptions about

[a] e-mail: `grabmayr@uni-tuebingen.de`

the pionic content of the nucleon. We found that all parameters of eq. (2) can be fixed by other experiments and are connected with the existence of pions in the nucleons. In order to disentangle shape and magnitude of G_E^n we propose the use of the parameter a' which is defined as $a_G = a' \cdot b_G$. The parameter b_G can be related to the pion electromagnetic form factor F_π and a' to the spectroscopic strength of the pions (number of pions) in the nucleon. With this prescription, reasonable parameters entering in eq. (2) are obtained supporting the proposed interpretation. Using "our" Galster-like parameterization we are also able to relate the data for the pion e.m. form factor F_π as provided by electroproduction experiments to the neutron electric form factor G_E^n. By this procedure, a high-quality representation of G_E^n can be obtained in the low-momentum transfer-region, where the direct double-polarization data are still not available and would have large corrections due to final-state interaction.
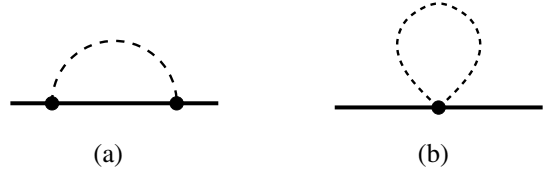
By now it is well established that the pion cloud plays an important role in understanding the variety of electromagnetic and hadronic properties of nucleons in the low-energy, nonperturbative region of QCD [17,18]. The coupling of the pion field to the nucleon quark core and the resulting pion loop (pion cloud) corrections are important ingredients of the so-called chiral quark models (χQM) [18] where the pions are the Goldstone bosons generated by spontaneous breaking of $SU(2)_R \times SU(2)_L$ chiral symmetry. Easily the scheme can be generalized to the octet of light pseudo-scalar mesons (π, K, η) as provided by $SU(3)_R \times SU(3)_L$. Formally, the pion cloud can be introduced into the nucleon structure by the perturbative expansion of the nucleon Fock space. This procedure is reflected in the two-component structure of the nucleon wave function $\Psi_N = (\Psi_{3q}, \Psi_{3q+\pi})$, where the first component, Ψ_{3q}, represents the bare nucleon consisting of valence quarks, and the second one, $\Psi_{3q+\pi}$, is the quark core dressed by a pion cloud which is mainly responsible for the soft physics. The presence of a soft pion cloud as an actual dynamical degree of freedom is crucial in understanding the neutron electric form factor G_E^n. In χQMs at the one-pion loop level, the neutron charge form factor is a first-order effect of the pion cloud and originates mainly from the Fock component of the neutron wave function consisting of a π^- cloud and a positively charged core of confined quarks. This physical picture gives a natural explanation of the nonvanishing charge-distribution inside the neutron which otherwise, like in the simplest version of nonrelativistic quark model (NRQM) with three valence quarks only, results in zero [17].

Consider the effective $SU(2)_R \times SU(2)_L$ Lagrangian of the χQM which can be written formally as [18]

$$\mathcal{L} = \mathcal{L}_\pi^{(2)} + \mathcal{L}_{\pi qq}^{(1)}, \qquad (3)$$

where the mesonic Lagrangian $\mathcal{L}_\pi^{(2)}$ of lowest order in the derivative expansion is given by the nonlinear σ model and the $\mathcal{L}_{\pi qq}^{(1)}$ is an effective pion-quark Lagrangian

$$\mathcal{L}_{\pi qq}^{(1)} = -\frac{1}{4 f_\pi^2} \bar\psi \gamma^\mu \boldsymbol{\tau} \psi [\boldsymbol{\pi} \times \partial_\mu \boldsymbol{\pi}] - \frac{f_{\pi qq}}{m_\pi} \bar\psi \gamma^\mu \gamma_5 \boldsymbol{\tau} \psi \partial_\mu \boldsymbol{\pi} \quad (4)$$

Fig. 1. One-pion loop self-energy diagrams. The intermediate state in (a) can be a nucleon or a Δ. The tadpole (Hartree) diagram in (b) vanishes due to its isospin structure.

where ψ and $\boldsymbol{\pi}$ are a quark and a pion field, respectively, and the coupling constant $f_{\pi qq}$ characterizes the strength of the pion-quark interaction. The coupling of the pion field to the core of confined quarks, eq. (4), results in pion loop corrections as provided by the self-energy pion loop diagrams shown in fig. 1 already on the hadronic level. Note that the underlying quark substructure of the diagrams is reflected in the appearance of hadronic form factors as shown by filled circles. The tadpole diagram (fig. 1(b)) vanishes due to its isospin structure and fig. 1(a) is characterized by the loop integral $-i\Sigma_\alpha(E)$ (see its explicit expression in ref. [18]), where the intermediate states α are a $N(939)$ or a $\Delta(1232)$. Figure 1(a) introduces the pionic degrees of freedom into the nucleon structure and mathematically requires the renormalization of the total nucleon wave function $|\Psi_N\rangle^R = Z_2^{-1/2}|\Psi_N\rangle$, where the constant Z_2 is given by

$$Z_2 \equiv 1 - \sum_\alpha \partial \Sigma_\alpha(E)/\partial E|_{E=M_N} \qquad (5)$$

and describes the probability of finding the "physical" nucleon in its bare three-quark valence Fock state. It also guarantees $^R\langle\Psi_N|\Psi_N\rangle^R = 1$. The value Z_2 can be related to the pionic content of the nucleon, namely to the pion spectroscopic factor, which represents the number of pions in the nucleon $S_\pi = \sum_\alpha S_\pi^\alpha = (Z_2 - 1)/Z_2$ or

$$S_\pi^\alpha = -\frac{1}{Z_2} \frac{\partial \Sigma_\alpha(E)}{\partial E}\bigg|_{E=M_N}. \qquad (6)$$

The explicit introduction of the additional degrees of freedom in the nucleon structure will change its properties as compared to expectations based on simple quark models in which the nucleon is described as a system of three valence quarks only. For example, the coupling of the e.m. field $\mathcal{A}^\mu$ to the conserved e.m. currents due to a quark charge $\mathcal{Q} = [1/3 + \tau_3]/2$ which is achieved by a photon-quark interaction

$$\mathcal{L}_{\gamma qq}^{(1)} = -e\, \mathcal{Q}\bar\psi\gamma^\mu\psi\mathcal{A}_\mu, \qquad (7)$$

should be supplemented by the coupling of the photon field to pions and is given by the $\gamma\pi$ interaction Lagrangian

$$\mathcal{L}_{\gamma\pi\pi}^{(2)} = -e\, [\boldsymbol{\pi} \times \partial^\mu \boldsymbol{\pi}]_3 \mathcal{A}_\mu; \qquad (8)$$
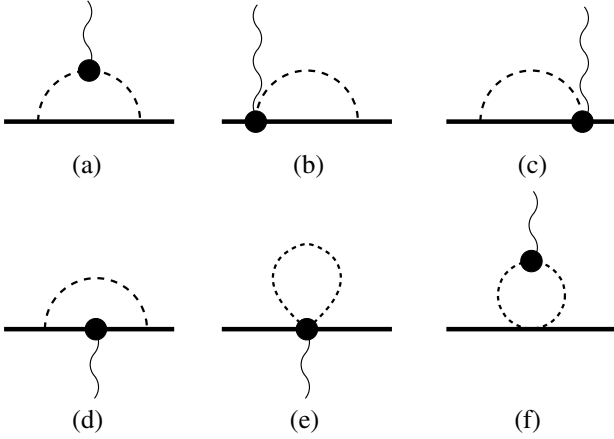
Fig. 2. E.m. currents at one-pion loop level.

with additional contact interactions obtained by a gauge transformation of the pion field of eq. (4) we get

$$\mathcal{L}_{\gamma\pi qq}^{(1)} = -e\,\frac{f_{\pi qq}}{m_\pi}\bar{\psi}\gamma^\mu\gamma_5[\boldsymbol{\tau}\times\boldsymbol{\pi}]_3\psi\mathcal{A}_\mu\,, \qquad (9)$$

$$\mathcal{L}_{\gamma\pi\pi qq}^{(1)} = -e\,\frac{1}{4f_\pi^2}\bar{\psi}\gamma^\mu[[\boldsymbol{\tau}\times\boldsymbol{\pi}]\times\boldsymbol{\pi}]_3\psi\mathcal{A}_\mu\,. \qquad (10)$$

Considering eqs. (7)-(10) at the one-pion loop level, the full set of diagrams responsible for the neutron charge form factor are shown in fig. 2. Since the bare quark core, eq. (7), and the "seagull" terms ($\sim\mathcal{O}(1/M_n)$) shown in fig. 2(b) and (c) do not contribute and since the tadpole contact graphs, fig. 2(e) and (f), cancel exactly, the leading-order contribution arises from two one-pion loop processes with γqq (fig. 2(d)) and $\gamma\pi\pi$ couplings (fig. 2(a)), respectively. Following to the standard Feynmann rules the e.m. current operators responsible for fig. 2(a) and (d) can be constructed and in the Breit frame, where $Q^2 = \boldsymbol{q}^2$, the resulting Sachs electric form factors of the neutron can be obtained as

$$G_{E_n}^{\gamma qq}(\boldsymbol{q}^2) = \frac{\tilde{G}(\boldsymbol{q}^2)}{Z_2}\sum_\alpha\mathcal{K}_{N\alpha}\int\frac{\mathrm{d}^3\boldsymbol{k}}{(2\pi)^3}\,\boldsymbol{k}^2 F^2(\boldsymbol{k}^2)\,\mathcal{C}_\alpha^{\gamma qq}(\boldsymbol{q},\boldsymbol{k}),$$
$$(11)$$

$$G_{E_n}^{\gamma\pi\pi}(\boldsymbol{q}^2) = -\frac{F_\pi(\boldsymbol{q}^2)}{Z_2}\sum_\alpha\mathcal{K}_{N\alpha}$$
$$\times\int\frac{\mathrm{d}^3\boldsymbol{k}}{(2\pi)^3}F(\boldsymbol{k}^2)F(\boldsymbol{k}'^2)\mathcal{C}_\alpha^{\gamma\pi\pi}(\boldsymbol{q},\boldsymbol{k},\boldsymbol{k}')\boldsymbol{k}\cdot\boldsymbol{k}', \quad (12)$$

where $\mathcal{K}_{N\alpha} = (f_{\pi qq}/m_\pi)^2\,C_{N\alpha}^2\chi^\alpha$ and $\boldsymbol{k}' = \boldsymbol{k}+\boldsymbol{q}$. The coefficients are calculated algebraically within the CQM and result in $\chi^N = 2$, $\chi^\Delta = -4/9$, $C_{NN} = 5/3$ and $C_{N\Delta} = 2\sqrt{2}$. $F_\pi(\boldsymbol{q})$ is the pion e.m. form factor and $F(\boldsymbol{k})$ is the nucleon axial form factor. Furthermore, $\tilde{G}(\boldsymbol{q}^2)$ in eq. (11) represents the electric form factor of the quark core. At the one-pion loop level the e.m. current operators as provided by fig. 2 involve a four-dimensional integration over the momentum k of the virtual pions. The momentum-dependent factors $\mathcal{C}_\alpha^{\gamma\pi\pi}(\boldsymbol{q},\boldsymbol{k},\boldsymbol{k}')$ and $\mathcal{C}_\alpha^{\gamma qq}(\boldsymbol{q},\boldsymbol{k})$ are the

result of the integration over k_0, which we perform analytically by closing the contour in the lower half of the complex plane. Equations (11) and (12) are exact and hold for any chiral quark model involving a cloud of pions. Instead of doing model calculations at this stage we proceed further by simplifying them. It can be shown that in the limit of low Q^2, eqs. (11) and (12) can be reduced to

$$\begin{Bmatrix} G_{E_n}^{\gamma qq}(\boldsymbol{q}^2) \\ G_{E_n}^{\gamma qq}(\boldsymbol{q}^2) \end{Bmatrix} = \left[\sum_\alpha\xi_\alpha S_\pi^\alpha\right]\begin{Bmatrix} \tilde{G}(\boldsymbol{q}^2) \\ -F_\pi(\boldsymbol{q}^2)F(\boldsymbol{q}^2) \end{Bmatrix}\,, \quad (13)$$

where S_π^α is given by eq. (6) and the spin-isospin factors are $\xi_N = 2/3$ and $\xi_\Delta = -1/3$. Here the pion e.m. form factor $F_\pi(\boldsymbol{q})$, the nucleon axial form factor $F(\boldsymbol{q})$ and the core electric form factor $\tilde{G}(\boldsymbol{q}^2)$ are the relevant ingredients which define the Q^2 behavior of the reduced form factors. The latter two are characteristics of the quark core. Their appearance is quite unique in all the quark models —they do not exist in effective Lagrangian approaches at hadronic level. The important feature of the CQM, at least for our considerations, is that the axial $F(\boldsymbol{q}^2)$ and electric $\tilde{G}(\boldsymbol{q}^2)$ form factors have the same functional form: $F(\boldsymbol{q}^2) = \tilde{G}(\boldsymbol{q}^2)$. We use this fact to recombine eqs. (13) as

$$G_E^n(\boldsymbol{q}^2) = \tilde{G}(\boldsymbol{q}^2)\left[1 - F_\pi(\boldsymbol{q}^2)\right]\sum_\alpha\xi_\alpha S_\pi^\alpha\,. \qquad (14)$$

Furthermore, as known from electroproduction experiments the pion e.m. form factor $F_\pi(\boldsymbol{q}^2)$ can be fitted up to a few GeV [19,20] by a monopole term

$$F_\pi(Q^2) = \Lambda_\pi^2/(\Lambda_\pi^2 + Q^2) = (1 + Q^2/\Lambda_\pi^2)^{-1}\,, \qquad (15)$$

with a cut-off mass $\Lambda_\pi^2 = 0.53$ GeV^2 [19,20]. Using eq. (15) the expression for G_E^n can be written alternatively

$$G_E^n(Q^2) = \sum_\alpha\xi_\alpha S_\pi^\alpha\cdot\left[\frac{Q^2/\Lambda_\pi^2}{1 + Q^2/\Lambda_\pi^2}\right]\tilde{G}(Q^2)\,. \qquad (16)$$

We define the two parameters a' and b as

$$b = 4M_n^2/\Lambda_\pi^2 \qquad\text{and}\qquad a' = \sum_\alpha\xi_\alpha S_\pi^\alpha\,. \qquad (17)$$

If we assume in addition that the quark core electric form factor is given by the dipole ansatz, $\tilde{G} = G_D$, we then arrive at a Galster-like formulation for G_E^n (cf. eq. (2)):

$$G_E^n(Q^2) = a'\,\frac{b\tau}{1 + b\tau}\,G_D(Q^2)\,, \qquad (18)$$

where $\tau = Q^2/4M_n^2$. Already at this level "our" Galster form decouples the parameters responsible for shape (b) and magnitude (a'), which reduces the uncertainty for b by about a factor 2 in the fits. Note that the form of $\tilde{G}$ is model dependent; however, its generalization to other hadronic models is straightforward. Presently, we have used the dipole form to make the direct correspondence with the Galster ansatz.
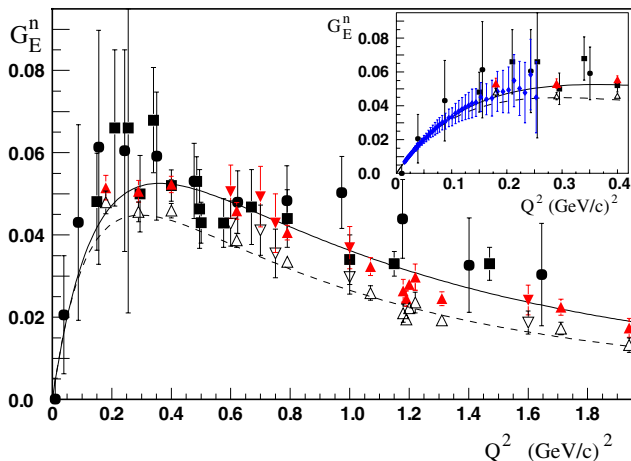
Fig. 3. The neutron electric G_E^n form factor. Squares: polarization data from ref. [14]. Circles: elastic electron-deuteron data [16]. Triangles: eq. (20) with pion data of refs. [19,20]; (open symbols: $\Lambda^2 = 0.71$ GeV^2, full symbols: $\Lambda^2 = 0.86$ GeV^2). The insert shows the low-Q^2 range with additional pion data [21].

a' in eqs. (17) and (18), which characterizes the spectroscopic strength of the pions in the nucleon, can be also fixed by imposing additional constraints coming from the experimental value of the neutron charge radius $\langle r^2 \rangle_n$. The latter is defined as the slope of $G_E^n(Q^2)$ for $Q^2 \to 0$, and applying this prescription to eq. (16) we obtain

$$\langle r^2 \rangle_n = -(6/\Lambda_\pi^2) \sum \xi_\alpha S_\pi^\alpha \quad \text{or} \quad a' = -\langle r^2 \rangle_n (\Lambda_\pi^2/6). \quad (19)$$

Assuming $\langle r^2 \rangle_n$ and F_π to be known, an even simpler expression for G_E^n emerges,

$$G_E^n(Q^2) = -\frac{\langle r^2 \rangle_n}{6} Q^2 F_\pi(Q^2) G_D(Q^2), \quad (20)$$

with no additional parameter. We mention that in eq. (20) all quantities responsible for the properties of the pion cloud are experimentally accessible. This fact can be used to obtain the G_E^n values directly from $\langle r^2 \rangle_n$ and F_π.

Inserting the experimental values for $\langle r^2 \rangle_n$ [9] and for F_π as extracted from electroproduction experiments [19, 20] directly into the above equation we obtain the data (open triangles) plotted in fig. 3. For comparison, G_E^n values selected by ref. [4] are given by squares and the evaluation of ref. [16] is presented by circles. The remarkable feature of the pion data is that they have smaller errors and that they lead to slightly smaller values for G_E^n above $Q^2 = 0.3$ GeV^2. In fig. 3 the full curve represents the fit to the G_E^n data [4,14] including the $\langle r^2 \rangle_n$ value, whereas the dashed curve represents the fit to the pion data with $\Lambda_D^2 = 0.71$ GeV^2 with reasonable χ^2 (table 1).

We note that, the use of $\Lambda_D^2 = 0.71$ GeV^2 in eq. (18) is not entirely correct as $\tilde{G}$ represents the core and not the extension of the total charge. Using parameters a' and b according to the above formulae, $\Lambda^2 = 0.86$ GeV^2 is obtained from a fit to the polarization data (third fit of table 1). The resulting curves from the first and third fit are

Table 1. Galster fits to G_E^n data.

Ref.	a'	b	$\Lambda^2/$GeV^2	$\chi^2/$n.d.o.f.
[4,14]	0.369 ± 0.008	4.69 ± 0.11	$0.71^{(a)}$	9.9/14
[19]	0.221 ± 0.002	8.21 ± 0.16	$0.71^{(a)}$	34.2/19
[4,14]	$0.26^{(a)}$	$6.65^{(a)}$	0.86 ± 0.04	9.7/15

$(^a)$ Fixed in the fit.

identical below $Q^2 = 2$ GeV^2 despite the different parameters. Using this $\Lambda^2 = 0.86$ GeV^2, which corresponds to a $\sqrt{\langle r^2 \rangle} = 0.74$ fm of the core, results in derived G_E^n values (full triangles in fig. 3) similar to the measured polarization data. The insert show the obtained G_E^n data for very low-Q^2 range where more pion data [21] have been added. In this momentum transfer region F_π can be understood to provide a model-independent input to G_E^n. Since $\tilde{G}$ is close to unity, G_E^n is considered to be parameter free at low Q^2. Interestingly, the G_E^n data from pion electroproduction fall right on top of the full curve. Clearly, the pion data can only account for the soft contributions; however they give a lower limit for G_E^n when using Λ_D. Parameter a' shows that the weighted sum of pion spectroscopic factors is in the range of 25% (table 1).

In summary, in this work we have obtained a theoretical justification of the phenomenologically successful Galster parameterization of the neutron electric form factor G_E^n. We have shown that the chiral (pion cloud) content in the nucleon structure is the crucial ingredient that leads under some approximations to a Galster-like Q^2-dependence of G_E^n. We found that all parameters of eq. (18), i.e. a' and b, can be fixed by other experiments and that they are connected with the existence of pions in the nucleons. The proposed parameterization of the G_E^n, eqs. (18) and (20), decouples the parameters responsible for shape (b) and magnitude (a') and allows to derive precise G_E^n data at low Q^2 where the direct measurements of G_E^n by double-polarization experiments require larger corrections factors due to the notorious final-state interactions.

We finally mention, that an analog prescription, eq. (20), can be set up for the strange electric form factors and the strange radius of the nucleon.

References

1. R. Hofstadter, R. Herman, Phys. Rev. Lett. **15**, 293 (1961); E.E. Chambers, R. Hofstadter, Phys. Rev. **103**, 1454 (1956).
2. E.J. Brash *et al.*, Phys. Rev. C **65**, 051001(R) (2001).
3. J.J. Kelly, Phys. Rev. C **66**, 065203 (2002).
4. J. Friedrich, T. Walcher, Eur. Phys. J. A **17**, 607 (2003).
5. Haiyan Gao, Int. J. Mod. Phys. E **12**, 1 (2003).

6. M.M. Kaskulov, P. Grabmayr, Phys. Rev. C **67**, 042201(R) (2003).
7. E. Fermi, L. Marschall, Phys. Rev. **72**, 1139 (1947).
8. L.L. Foldy, Phys. Rev. **87**, 688; 693 (1952).
9. S. Kopecky *et al.*, Phys. Rev. C **56**, 2220 (1997).
10. N. Isgur, Phys. Rev. Lett. **83**, 272 (1999).
11. D.B. Leinweber, A.W. Thomas, R.D. Young, Phys. Rev. Lett. **86**, 5011 (2001).
12. S. Galster *et al.*, Nucl. Phys. B **32**, 221 (1971).
13. S. Platchkov *et al.*, Nucl. Phys. A **570**, 740 (1990).
14. G_E^n data compiled in table 1 of ref. [4].
15. P. Grabmayr, A.J. Buchmann, Phys. Rev. Lett. **86**, 2237 (2001).
16. R. Schiavilla, I. Sick, Phys. Rev. C **64**, 041002 (2001).
17. G.A. Miller, Phys. Rev. C **66**, 032201 (2002).
18. A.W. Thomas, W. Weise, *The Structure of the Nucleon* (Wiley-VCH, Berlin, 2001).
19. C.J. Bebek *et al.*, Phys. Rev. **17**, 1693 (1978).
20. J. Volmer *et al.*, Phys. Rev. Lett. **86**, 1713 (2001).
21. S.R. Amendolia *et al.*, Nucl. Phys. B **277**, 168 (1986).